USCAP

ARTICLE

Early infiltrating macrophage subtype correlates with late-stage phenotypic outcome in a mouse model of hepatorenal fibrocystic disease

Kurt A. Zimmerman[1,2], Cheng J. Song[1], Ernald J. G. Aloria[1], Zhang Li[1], Juling Zhou[3], Sarah J. Bland[2], Alex Yashchenko[2], David K. Crossman[4], Michal Mrug[3,5] and Bradley K. Yoder[1]✉

Hepatorenal fibrocystic disease (HRFCD) is a genetically inherited disorder related to primary cilia dysfunction in which patients display varying levels of fibrosis, bile duct expansion, and inflammation. In mouse models of HRFCD, the phenotype is greatly impacted by the genetic background in which the mutation is placed. Macrophages are a common factor associated with progression of HRFCD and are also strongly influenced by the genetic background. These data led us to hypothesize that macrophage subtypes that change in relation to the genetic background are responsible for the variable phenotypic outcomes in HRFCD. To test this hypothesis, we utilized a mouse model of HRFCD (*Ift88*^{Orpk} mice) on the C57BL/6 and BALB/c inbred backgrounds that have well-documented differences in macrophage subtypes. Our analyses of infiltrating macrophage subtypes confirm that genetic strain influences the subtype of infiltrating macrophage present during normal postnatal liver development and in *Ift88*^{Orpk} livers (Ly6c^{lo} in C57BL/6 vs Ly6c^{hi} in BALB/c). Each infiltrating macrophage subtype was similarly associated with a unique phenotypic outcome as analysis of liver tissue shows that C57BL/6 *Ift88*^{Orpk} mice have increased bile duct expansion, but reduced levels of fibrosis compared to BALB/c *Ift88*^{Orpk} livers. RNA sequencing data suggest that the ability to infiltrate macrophage subtypes to influence the phenotypic outcome may be due to unique ligand-receptor signaling between infiltrating macrophages and cilia dysfunctional biliary epithelium. To evaluate whether specific macrophage subtypes cause the observed phenotypic divergence, we analyzed the liver phenotype in BALB/c *Ift88*^{Orpk} mice on a CCR2−/− background. Unexpectedly, the loss of Ly6c^{hi} macrophages, which were strongly enriched in BALB/c *Ift88*^{Orpk} mice, did not significantly alter liver fibrosis. These data indicate that macrophage subtypes may correlate with HRFCD phenotypic outcome, but do not directly cause the pathology.

Laboratory Investigation (2021) 101:1382–1393; https://doi.org/10.1038/s41374-021-00627-0

INTRODUCTION

Hepatorenal fibrocystic disease (HRFCD) is a common inherited genetic disease that affects approximately 1:500 people and is characterized by cysts and fibrosis in the kidney and liver [1–3]. This disease is caused by mutations in proteins required for normal cilia function (*Pkhd1*, *Pkd1*, or *Pkd2*). Even when caused by a common genetic mutation, patients with HRFCD have varying disease severity and progression that is thought to be caused by environmental and genetic modifiers [4–7]. The phenotypic variability observed in patients can be mimicked using HRFCD mouse models inbred on different genetic backgrounds [8]. Importantly, there is a strong association between genetic background and immune cell subtypes (and their gene expression profiles) in mice and humans raising the possibility that genetic strain-driven alterations in immune cells may be contributing to the phenotype variability [9–11].

Current data indicate a strong association between macrophages and HRFCD [12–18]. The functional importance of macrophages in HRFCD is well established as general macrophage depletion reduces liver and kidney fibrocystic disease [16–18]. In these studies, the data suggested that M2-like macrophages were predominantly responsible for promoting cyst progression as macrophage depletion (using liposomal clodronate) during periods of maximal M2-like macrophage accumulation significantly attenuated cystic disease [19]. Further, inhibition of Arg1 activity, typically associated with M2-like macrophages, reduced cystic disease suggesting that distinct macrophage subtypes control the phenotypic outcome in the kidney [19]. However, in vivo, macrophages are more clearly defined based on their ontological origin (infiltrating vs resident) than on M1/M2 polarization status [20]. Infiltrating macrophages (CD11b^{hi}, F4/80^{lo} cells) originate from the hematopoietic lineage in the adult bone marrow and are recruited to tissues in response to injury or infection through cytokines, such as CCL2, binding to its cognate receptor (CCR2) expressed on the immune cell [21–25]. Previous work from our lab demonstrated the importance of infiltrating

[1]Department of Cell, Developmental, and Integrative Biology, University of Alabama at Birmingham, Birmingham, AL, USA. [2]Department of Internal Medicine, Division of Nephrology, University of Oklahoma Health Sciences Center, Oklahoma City, OK, USA. [3]Department of Medicine, Division of Nephrology, University of Alabama at Birmingham, Birmingham, AL, USA. [4]Department of Genetics, University of Alabama at Birmingham, Birmingham, AL, USA. [5]Department of Veterans Affairs Medical Center, University of Alabama at Birmingham, Birmingham, AL, USA. ✉email: byoder@uab.edu

Received: 16 March 2021 Revised: 7 June 2021 Accepted: 7 June 2021
Published online: 22 June 2021

macrophages in regulating fibrocystic liver disease in *Ift88*^{Orpk} FVB mice [26]. Further supporting the idea that infiltrating macrophages are pathogenic cells in HRFCD, two recent findings show that renal tubule-derived *Ccl2* promotes macrophage accumulation and cyst formation in mouse models of cystic kidney disease [27, 28]. Surprisingly, pharmacological inhibition of CCL2 using bindarit did not reduce cyst formation in the kidney or liver of PCK rats, although the effect of bindarit on macrophage number in the kidney and liver was moderate [29]. Collectively, these data suggest that the variability in phenotypic outcome observed in human patients and in mouse models on different genetic backgrounds may be influenced by the type of macrophage present in the tissue.

Herein, we set out to define the association between infiltrating macrophage subtypes and the hepatic phenotypes observed in an HRFCD mouse model caused by cilia dysfunction (*Ift88*^{Orpk}). Our data indicate that genetic strain strongly influences the subtype of infiltrating macrophage present in the liver during normal postnatal development (Ly6c^{hi} infiltrating macrophage in BALB/c vs Ly6c^{lo} infiltrating macrophage in C57BL/6) and in *Ift88*^{Orpk} mice. Further, we compared infiltrating macrophage subtypes relative to the phenotypic outcomes in *Ift88*^{Orpk} mice on these genetic backgrounds. While our data indicate there is a strong correlation between the hepatic phenotypes and the infiltrating macrophage subtype, we find that these associations are not causative of the phenotypic variability.

MATERIALS AND METHODS

Mice

Two, four, and eight week old C57BL/6J and BALB/c *Ift88*^{Tg737Rpw} (hereafter referred to as *Ift88*^{Orpk}) male and female mice were bred in-house. Animals were maintained in Association for Assessment and Accreditation of Laboratory Animal Care International-accredited facilities in accordance with Institutional Animal Care and Use Committee regulations at the University of Alabama at Birmingham (UAB). For all experiments, littermates were used as control mice. BALB/c *Ift88*^{Orpk} CCR2−/− mice were obtained by crossing BALB/c *Ift88*^{Orpk} mice with BALB/c CCR2−/− mice (generous gift of Dr. Nancy McNamara, University of California-San Francisco). Mice were fed a Purina High Energy Mouse Diet (Catalog #: 5LJ5) ad libitum.

Harvesting, fixation, and tissue processing

Mice were anesthetized with avertin (2,2,2-tribromoethyl alcohol, Sigma) and transcardially perfused with 20 mL of D-PBS. Following perfusion, mouse livers were weighed and separated into individual lobes. One lobe was used for flow cytometry, two lobes were snap-frozen in liquid nitrogen, one lobe was immersion fixed in 4% (wt/vol) paraformaldehyde 1 h at room temperature followed by cryoprotection in 30% (wt/vol) sucrose overnight at 4 °C, and one lobe was fixed in PFA overnight, dehydrated in 70% ethanol overnight, and embedded in paraffin. Paraffin-embedded tissue was sectioned at 5 µm and stained using hematoxylin and eosin (H&E). Picrosirius red staining was performed by the UAB Comparative Pathology Laboratory.

Picrosirius red quantification was performed using ImageJ software. Five 10X objective images from 2 to 8-week old C57BL/6 and BALB/c *Ift88*^{Orpk} mice were used for the analysis. For each time point, a threshold value in which red staining was minimally detected in periportal regions in control mice by Image J software was determined and applied to all samples. Data from individual images were combined to determine the average for each mouse.

Quantification of expanded biliary structures was done using H&E stained sections and ImageJ software. Five 10X objective images from 2 and 8-week old C57BL/6 and BALB/c *Ift88*^{Orpk} mice were used for the analysis. For each time point, a threshold value in which open biliary structures were considered to be holes was determined and applied to all samples. Non-epithelial structures were identified by a pathologist who was blinded to the groupings. Data collected from individual images were combined to determine the average for each mouse.

Flow cytometry

Following perfusion with PBS, one lobe of the liver was removed and put into RPMI 1640 on ice. Harvested liver tissue was mechanically disrupted through a 70-µm mesh (Falcon; BD Biosciences) yielding single-cell suspensions. Cells were centrifuged at 1300 rpm (500 × *g*) for 5 min and red blood cells lysed using ACK red blood cell lysis buffer (Quality Biological; 10128-802) at 37 °C for 5 min. Cells were centrifuged at 1300 rpm (220 × *g*), resuspended in 1 ml of 1% BSA containing Fc blocking solution (dilution 1:200), and incubated for 30 min on ice. Following cell counting with trypan blue, approximately 2 million live cells were stained for 30 min at room temperature with conjugated primary antibodies including PE rat anti-mouse CD45 (Catalog #: 12-0451-81, 30-F11, ThermoFisher), eFluor®450 rat anti-mouse F4/80 (Catalog #:48-4801, BM8, eBioscience), APC rat anti-mouse CD11b (Catalog #:17-0112, M1/70, eBioscience), APC/Cy7 rat anti-mouse Gr-1 (Catalog #:557661, RB6-8C5, BD Pharmingen), and PerCP-cy 5.5 rat anti-mouse Ly6c (Catalog #:560525, clone: AL-21, BD Pharmingen). Cells were washed with 1% BSA, centrifuged at 1300 rpm, and fixed with 2% PFA at room temperature for 30 min. Cells were washed with 1% BSA, centrifuged at 1300 rpm, and resuspended in 1X PBS. After immunostaining, cells were analyzed on a BD LSRII flow cytometer. Data analysis was performed using FlowJo v10 software.

Fluorescence-activated cell sorting of cholangiocytes and macrophages for RNA sequencing

For flow sorting of individual cell populations from the whole liver, tissue was harvested and digested in RPMI containing 0.5 mg/ml collagenase with 100 U/ml DNase type I for 30 min at 37 °C with agitation. Single-cell suspensions were obtained and cells were stained as described above. For isolation of cholangiocytes, we used dolichos biflorus agglutinin (DBA) (RL-1032, Vector Laboratories), a well-established, cell surface marker of bile duct cholangiocytes [30]. Cells were sorted into individual tubes containing buffer RLT (Catalog #:74104 Qiagen, Hilden, Germany) to lyse the cells. Ultrapure RNA was isolated using the RNeasy kit (Qiagen, Hilden, Germany) following the manufacturer's protocol. The quality of RNA was determined using the Agilent 2100 bioanalyzer and only used if the RNA integrity number was above 7. We combined an equal amount of RNA from 6 to 8 individual mice per genotype (equal number of males and females) for RNA sequencing studies. Thus, the RNA sequencing data presented is an average of 6–8 biological replicates per group. The NEBNext mRNA library prep kit for Illumina with ribosome reduction was used to generate the cDNA library, which was subsequently sequenced using Illumina Next-Seq500 with paired-end 75 bp sequencing and aligned to the University of California, Santa Cruz (UCSC) GRCm38/mm10 reference genome using the STAR software package [31]. For each sample, at least 25 million reads were obtained. Following alignment, HTSeq-count (version 0.9.1) was used to count the number of reads mapping to each gene [32]. Fragments per kilobase of transcript per million mapped reads (FPKM) and pairwise differential expression were calculated using the Cufflinks suite (https://github.com/cole-trapnell-lab/cufflinks) and HTSeq-Count/DESeq2 was used to identify the most highly variable genes between groups.

RNA isolation from whole liver tissue and qRT-PCR

For qRT-PCR analysis of whole liver tissue, snap-frozen liver samples were thawed and ~25–50 mg of tissue was minced and disassociated in TRIzol (Thermo-Fisher, Waltham, MA). The tissue was homogenized using a 22 gauge needle followed by removal of tissue debris by centrifugation at 14,000 rpm for 5 min. The supernatant was removed, RNA was isolated, transcribed into cDNA, and qRT-PCR performed using TaqMan real-time PCR. The following probes were used: Col3a1 (Mm01254476_m1), Col1a2 (Mm00483937_m1), Krt19 (Mm00492980_m1), and Hprt (Mm00446968_m1).

Statistics

Data were presented as mean ± SEM. ANOVA and Student *t*-tests were used for statistical analysis, and differences were considered significant for *P* values less than 0.05. Outliers were excluded based on the Grubbs outlier test. *$P < 0.05$, **$P < 0.01$, ***$P < 0.001$, ****$P < 0.0001$

RESULTS

Infiltrating macrophage subtype and gene expression are influenced by genetic strain

To determine whether genetic strain influences infiltrating macrophage subtypes, we performed flow cytometry analysis of infiltrating macrophages isolated from the liver of C57BL/6 and BALB/c inbred mice under uniform environmental conditions. For

these studies, we performed flow cytometry analysis at 2, 4, and 8 weeks of age to understand how infiltrating macrophage subtypes change as a function of time. Infiltrating macrophages were further sub-gated based on differential expression of Ly6c, a cell surface protein previously reported to be associated with the rate of fibrotic disease in the liver (Ly6c^{hi} macrophages promote fibrosis) [33]. Our data show that the absolute number (as determined by the percentage of the total, live, single cells in the liver) of Ly6c^{hi} infiltrating macrophages was not different between groups at any time point (Fig. 1A, B). In contrast, livers from C57BL/6 mice had a significant increase in the number of Ly6c^{lo} infiltrating macrophages compared to BALB/c livers at all time points (Fig. 1A, B). Analysis of Ly6c^{hi}:Ly6c^{lo} ratio in both strains indicates that the majority of infiltrating macrophages in wild type (WT) BALB/c livers at 2, 4, and 8 weeks of age are Ly6c^{hi} (~70% Ly6c^{hi}) whereas C57BL/6 livers have an approximately equal distribution of Ly6c^{hi} and Ly6c^{lo} macrophages during the same time period (Fig. 1A, C). The altered ratio of Ly6c^{hi}:Ly6c^{lo} infiltrating macrophages across time points was driven by differences in the total number of Ly6c^{lo} infiltrating macrophages.

Along with the quantity and subset distribution of infiltrating macrophages, we evaluated whether there were differences in gene expression when comparing Ly6c^{hi} and Ly6c^{lo} infiltrating macrophages across genetic strains. Bulk RNA sequencing analysis was performed on WT Ly6c^{hi} and Ly6c^{lo} macrophages isolated from liver tissue of C57BL/6 and BALB/c mice at 4 weeks of age. Heatmap analysis and hierarchical clustering of the top 200 differentially expressed genes (DEGs) indicate that Ly6c^{lo} and Ly6c^{hi} infiltrating macrophages segregate together independent of genetic strain (Fig. 1D). A closer examination of macrophage-associated genes in each population revealed that expression of genes associated with extracellular matrix production and fibrosis including *Tgfb1, Fn1*, and *Thbs1* are increased in BALB/c Ly6c^{hi} macrophages compared to C57BL/6 Ly6c^{hi} macrophages (Fig. 1E). We also observed increased expression of antigen presentation and processing genes (*H2-Aa, Cd74, Itgax*) in BALB/c Ly6c^{lo} infiltrating macrophages compared to their C57BL/6 counterparts (Fig. 1E). Pathway analysis of genes enriched in infiltrating macrophages from each strain reveals that BALB/c infiltrating macrophages have an enrichment of genes associated with cytokine production and wound healing while C57BL/6 infiltrating macrophages have an enrichment of genes associated with phagocytosis and endosome formation (Fig. 1F). These data indicate that the ratio and gene expression of Ly6c^{hi} and Ly6c^{lo} infiltrating macrophages is different between genetic strains and thus, could differentially influence disease progression in *Ift88*^{Orpk} mice.

Genetic strain influences infiltrating macrophage recruitment in *Ift88*^{Orpk} mice

To address how infiltrating macrophage subtypes changed in the context of HRFCD, we analyzed infiltrating macrophages in the *Ift88*^{Orpk} mouse model of HRFCD by flow cytometry. *Ift88*^{Orpk} mice have hypomorphic levels of *Ift88* leading to short, malformed, dysfunctional primary cilia and HRFCD [2]. These analyses were done on mice at 2 and 4 weeks of age in order to understand how early changes in infiltrating macrophage subtype recruitment correlated with late-stage disease. In 2 and 4-week old mice, we did not observe any significant difference in the number of Ly6c^{lo} macrophages in either *Ift88*^{Orpk} strain compared to controls at any time point (Fig. 2A–D). In contrast, there was a significant increase in the number of Ly6c^{hi} infiltrating macrophages in BALB/c *Ift88*^{Orpk} livers compared to C57BL/6 *Ift88*^{Orpk} and BALB/c control livers (Fig. 2A–D). Similar to their WT counterparts, the ratio of Ly6c^{hi}:Ly6c^{lo} infiltrating macrophages was increased in BALB/c *Ift88*^{Orpk} mice compared to C57BL/6 *Ift88*^{Orpk} mice (Fig. 2E, F). Since Ly6c^{hi} infiltrating macrophages in the liver are associated with inflammation and fibrosis and Ly6c^{lo} infiltrating macrophages are associated with tissue repair and matrix degradation [33], our data suggest that BALB/c mice may be more prone to developing hepatic fibrosis due to the increased proportion of Ly6c^{hi} infiltrating macrophages while C57BL/6 mice may be resistant to hepatic fibrosis due to the increased proportion of Ly6c^{lo} infiltrating macrophages in the liver.

Infiltrating macrophage subtypes correlate with the severity of biliary hyperplasia and fibrosis in *Ift88*^{Orpk} mice

To test the hypothesis that differences in the ratio of infiltrating macrophage subtypes at early stages of disease correlate with late-stage phenotypic outcome, we analyzed the liver phenotype across the two inbred strains at 2, 4, and 8 weeks of age. H&E staining of 2-week-old *Ift88*^{Orpk} liver sections showed that the liver pathology and severity of biliary hyperplasia (as measured by bile duct area/portal area) was similar between the two genetic strains at this time point (Fig. 3A, B). To confirm a similar biliary pathology between strains at 2 weeks of age, we performed qRT-PCR for *Krt19*, a marker of bile duct cholangiocytes [34], on whole liver tissue isolated from control and *Ift88*^{Orpk} mice on the C57BL/6 and BALB/c backgrounds. Our data show that there is no difference in the expression of *Krt19* mRNA in 2-week-old *Ift88*^{Orpk} mice between genetic strains, confirming our histological analyses (Fig. 3C). In contrast to what was observed in 2-week old *Ift88*^{Orpk} mutants, H&E staining of 8-week old mice shows the expansion of biliary regions in all *Ift88*^{Orpk} mice with C57BL/6 *Ift88*^{Orpk} mice having increased biliary hyperplasia compared to BALB/c *Ift88*^{Orpk} mice (Fig. 3A, B). In agreement with these data, analysis of whole liver mRNA shows that *Krt19* expression was higher in 8-week old C57BL/6 *Ift88*^{Orpk} mice compared to 8-week old BALB/c *Ift88*^{Orpk} mice (Fig. 3C). Four-week-old mice appear to have an intermediate phenotype in both strains.

Since patients with HRFCD often develop severe hepatic portal fibrosis, we also analyzed fibrosis in C57BL/6 and BALB/c mice by performing qRT-PCR analysis of *Col1a2* and *Col3a1* from whole liver tissue isolated at 2, 4, and 8 weeks of age followed by confirmation of RNA data using picrosirius red staining and quantification. Similar to our previous finding in *Ift88*^{Orpk} FVB mice [26], 2 weeks old C57BL/6 and BALB/c *Ift88*^{Orpk} mice do not have increased levels of the extracellular matrix genes *Col1a2 and Col3a1* or picrosirius red positive area compared to control mice (Fig. 4A–D) [26]. In contrast, analysis of 4-week old *Ift88*^{Orpk} mice shows that BALB/c *Ift88*^{Orpk} mice have a significant increase in *Col1a2* and *Col3a1* gene expression compared to C57BL/6 *Ift88*^{Orpk} mice and BALB/c control mice (Fig. 4A, B). Increased expression of *Col3a1* was also observed in 8-week old BALB/c *Ift88*^{Orpk} mice compared to 8-week old *Ift88*^{Orpk} C57BL/6 and BALB/c control mice although not to a significant level (Fig. 4B). The increased level of fibrosis in BALB/c *Ift88*^{Orpk} mice compared to C57BL/6 *Ift88*^{Orpk} mice was confirmed using picrosirius red staining and quantification (Fig. 4C, D). Collectively, these data indicate that C57BL6 mice have increased biliary hyperplasia while BALB/c *Ift88*^{Orpk} mice have increased periportal fibrosis.

Genetic strain influences infiltrating macrophage gene expression in *Ift88*^{Orpk} mice

To understand how infiltrating macrophage subtypes may be influencing phenotypic outcomes in the liver of *Ift88*^{Orpk} mice, we performed heat map analysis of RNA sequencing data from Ly6c^{hi} and Ly6c^{lo} infiltrating macrophages that were isolated from WT and *Ift88*^{Orpk} mice on the C57BL/6 and BALB/c backgrounds. Sequencing and analyses were done on 4-week old mice with intermediate phenotypes so that we could identify changes in infiltrating macrophage gene expression prior to the presence of severe disease. A broad comparison of gene expression between C57BL/6 and BALB/c WT and *Ift88*^{Orpk} Ly6c^{hi} (top) and Ly6c^{lo} (bottom) infiltrating macrophages indicates that *Ift88*^{Oprk} mice

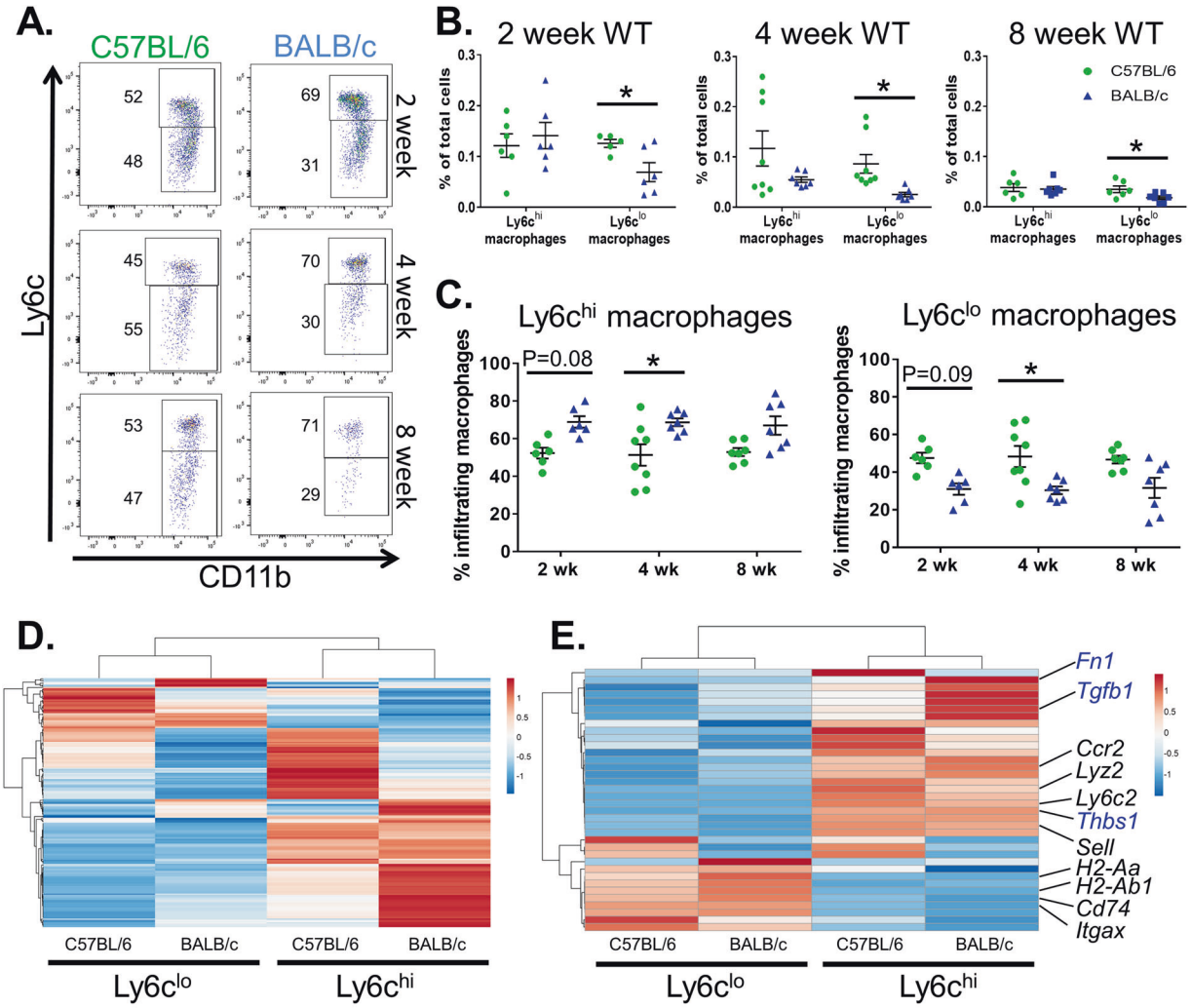

F.

	Pathway	Log P value	Genes
BALB/c	Regulation of defense response	-12.306	*Irf7, Fos, Ltf*
	Regulation of cytokine production	-11.656	*Il6ra, Csf1r, Cd74*
	Response to wounding	-10.098	*Thbs1, Fn1, Tgfb1, C3*
C57BL/6	Neutrophil degranulation	-15.177	*H2-K1, Cybb, Cd44*
	Phagosome	-11.73	*Coro1a, H2-Eb1, Clec7a*
	Endocytosis	-10.633	*Hspa8, Il2rb, Cd36*

Fig. 1 Genetic strain influences the subtype of infiltrating macrophage found in the liver during postnatal development. **A** Representative flow cytometry images showing Ly6c expression in infiltrating macrophages from 2, 4, and 8-week old WT C57BL/6 and BALB/c mice. **B** Quantification of the number of each cell type as a percentage of total cells for each time point is shown as average ± SE. $N =$ 6–10 mice. *$P < 0.05$. **C** Quantification of the percentage of infiltrating macrophages expressing high (left) or low (right) levels of Ly6c is shown for each genetic strain at the indicated time points. Data are shown as the mean ± SE. *$P < 0.05$. **D** Heatmap of RNAseq data obtained from 4-week old WT C57BL/6 and BALB/c Ly6c^{hi} and Ly6c^{lo} macrophages isolated from the liver showing the top 200 DEGs. **E** Heatmap analysis of macrophage-specific genes in WT C57BL/6 and BALB/c macrophages isolated from the liver. **F** List of pathways enriched in BALB/c and C57BL/6 infiltrating macrophages based on RNAseq analyses.

have several DEGs compared to their respective WT controls (Fig. 5A). Since C57BL/6 *Ift88*^{Orpk} mice have an increased ratio of Ly6c^{lo} infiltrating macrophages and BALB/c *Ift88*^{Orpk} mice have an increased ratio of Ly6c^{hi} infiltrating macrophages, we performed a GO pathway analysis of genes that were enriched in Ly6c^{lo} macrophages from C57BL/6 *Ift88*^{Orpk} mice and Ly6c^{hi} macrophages from BALB/c *Ift88*^{Orpk} mice to gain insight into their function. Our data show that Ly6c^{lo} macrophages isolated from C57BL/6 *Ift88*^{Orpk} mice have an enrichment of genes associated with the vascular wall, angiogenesis, and endothelial development (green arrows, Fig. 5B). We focused on these biological processes because several of the genes found within, including *Vegf*, promote cholangiocyte proliferation and bile duct expansion in the liver, thereby matching our observed liver pathology in these mice [35]. In contrast, Ly6c^{hi} macrophages from BALB/c *Ift88*^{Orpk} mice have enrichment of genes associated with the inflammatory response, cytokine production, and response to wounding, similar to their WT counterparts (blue arrows, Fig. 5B).

To further investigate how infiltrating macrophage subtypes may be influencing phenotypic outcome (i.e., proliferation-dependent bile duct expansion or fibrosis), we analyzed the expression of specific cytokines that are known to promote either cholangiocyte proliferation and bile duct expansion or extracellular matrix production and fibrosis in infiltrating macrophage

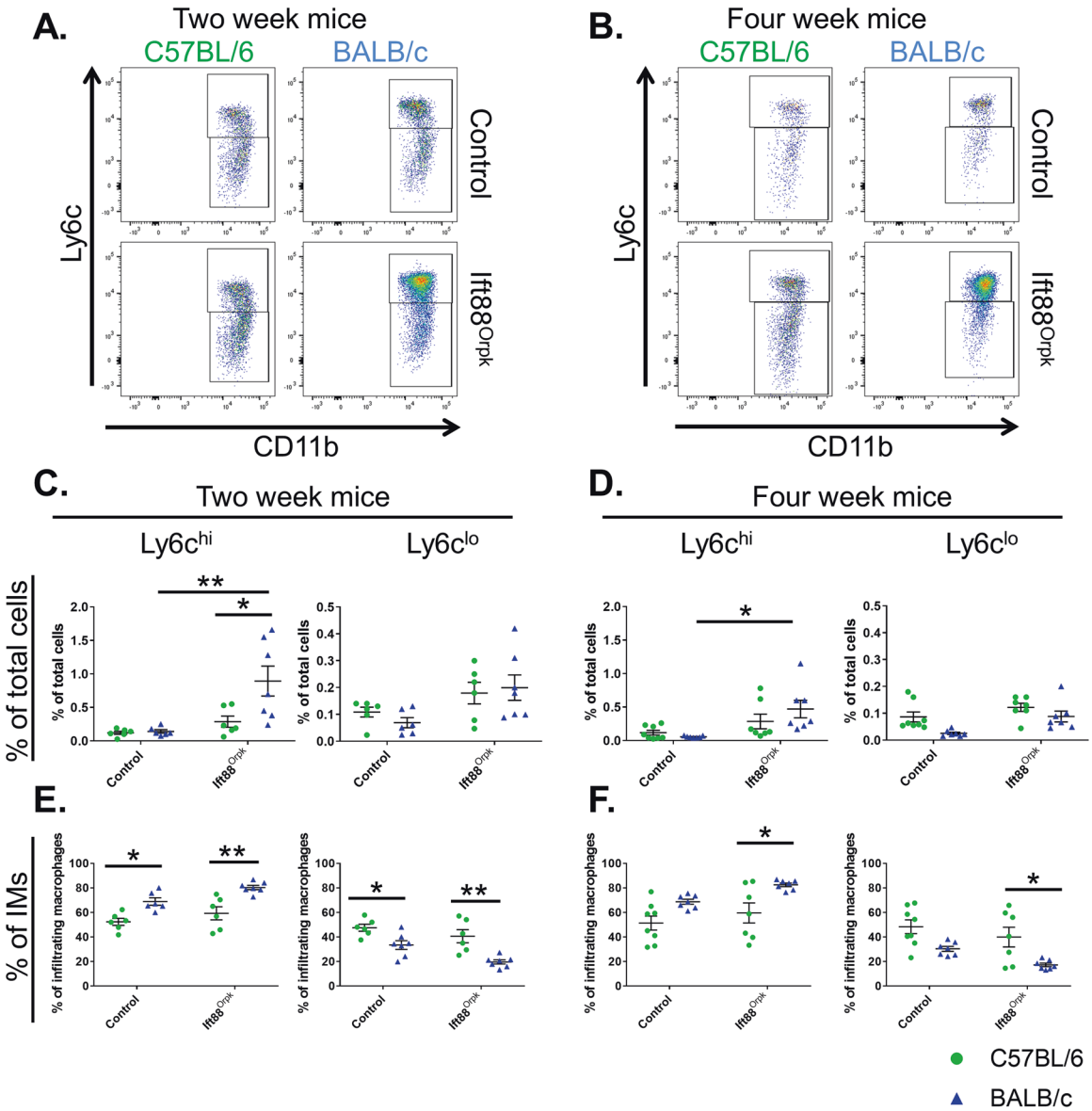

Fig. 2 Accumulation of infiltrating macrophage subtype in *Ift88*^{Orpk} mice is influenced by genetic strain. A, **B** Representative flow cytometry plots of Ly6c^{hi} and Ly6c^{lo} macrophages from (**A**) 2-week old or (**B**) 4-week old control and *Ift88*^{Orpk} C57BL/6 and BALB/c mice. **C**, **D** Quantification of the number of Ly6c^{hi} and Ly6c^{lo} infiltrating macrophages as a percentage of total cells in (**C**) 2-week old and (**D**) 4-week old livers. Data are plotted as the average ± SE. *$P < 0.05$ **$P < 0.01$. **E**, **F** Quantification of the percentage of infiltrating macrophages expressing high (left) or low (right) levels of Ly6c is shown for each genetic strain at (**E**) 2 and (**F**) 4 weeks of age. Data are shown as the mean ± SE. *$P <$ 0.05; **$P < 0.01$.

subtypes. Our analysis shows that Ly6c^{lo} macrophages from C57BL/6 WT and *Ift88*^{Orpk} mice have increased *Vegfc* transcripts compared to their Ly6c^{hi} counterparts whereas expression of other proliferative cytokines was minimal in these cells and virtually absent in Ly6c^{hi} macrophages (Fig. 5C). Analysis of pro-fibrotic growth factor gene expression reveals that BALB/c Ly6c^{hi} and Ly6c^{lo} WT and *Ift88*^{Orpk} infiltrating macrophages expressed these genes (Fig. 5D). However, expression of *Tgfb1*, a gene associated with extracellular matrix production and fibrosis in the liver [36, 37], was enriched in Ly6c^{hi} infiltrating macrophages compared to Ly6c^{lo} macrophages (Fig. 5D).

Genetic strain influences epithelial cell response to environmental cytokines in *Ift88*^{Orpk} mice

In these studies, we also analyzed how ciliated, bile duct epithelial cells (cholangiocytes) respond to alterations in environmental cytokines by performing RNA sequencing and analysis of cholangiocytes isolated from 4-week-old WT and *Ift88*^{Orpk} mice on the C57BL/6 and BALB/c background. Our data identified several changes in gene expression patterns between control and *Ift88*^{Orpk} cholangiocytes on both the C57BL/6 and BALB/c background (Fig. 6A). Pathway analysis of the genes that were enriched in cholangiocytes isolated from each *Ift88*^{Orpk} strain shows that C57Bl/6 *Ift88*^{Orpk} cholangiocytes have an enrichment of genes associated with VEGFR signaling pathways (green arrows, Fig. 6B) whereas cholangiocytes isolated from BALB/c *Ift88*^{Orpk} mice have an enrichment of genes associated with extracellular matrix organization and response to wounding (blue arrows, Fig. 6B). VEGFR signaling is known to promote bile duct expansion in the liver [35], which is consistent with our data showing that C57BL/6 mice have enhanced bile duct pathology and increased *Vegfc* transcripts in Ly6c^{lo} infiltrating macrophages.

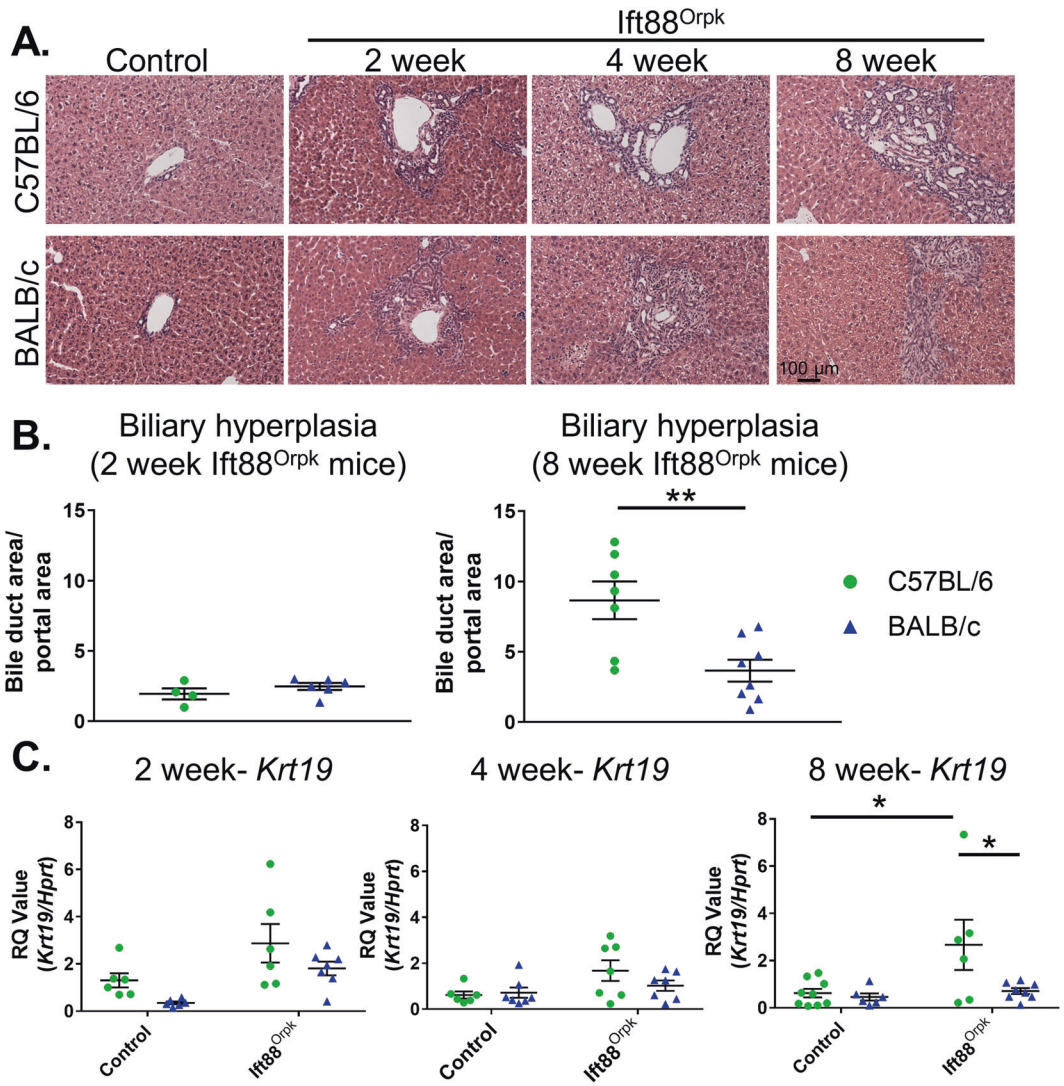

Fig. 3 C57BL/6 *Ift88*^{Orpk} mice have increased bile duct expansion in the liver compared to BALB/c *Ift88*^{Orpk} mice. A Control and *Ift88*^{Orpk} livers were harvested at the indicated time points and stained with hematoxylin and eosin. A representative 10X objective image from each mouse is shown. $N = 5–8$ per group. **B** Quantification of biliary hyperplasia (bile duct area/portal area) in 2 and 8-week-old C57BL/6 and BALB/c *Ift88*^{Orpk} mice are shown as average ± SE. $^{**}P < 0.01$. **C** qRT-PCR analysis of *Krt19* mRNA in whole liver tissue from 2, 4, and 8-week-old control and *Ift88*^{Orpk} C57BL/6 and BALB/c mice. Data are shown as the average ± SE. $^{*}P < 0.05$.

To further investigate ligand:receptor crosstalk between infiltrating macrophage subtypes and cholangiocytes that may cause the divergent phenotypic outcome in *Ift88*^{Orpk} mice from each genetic background, we analyzed gene expression of receptors known to drive extracellular matrix production, mesenchymal transition, and cholangiocyte proliferation in the RNA sequencing data. Analysis of pro-fibrotic growth factor receptor expression shows that C57BL/6 *Ift88*^{Orpk} cholangiocytes have decreased *Fgfr2* and *Met* expression compared to C57BL/6 WT cholangiocytes (Fig. 6C). In contrast, *Ift88*^{Orpk} BALB/c cholangiocytes have increased expression of multiple pro-fibrotic growth factor receptors including *Fgfr2, Tgfbr1, Pdgfrb*, and *Pdgfra* compared to WT controls (Fig. 6C). Notably, the ligand for *Tgfbr1* (*Tgfb1*) was specifically enriched in Ly6c^{hi} infiltrating macrophages from BALB/c *Ift88*^{Orpk} mice suggesting crosstalk between these cell types. We also observed increased gene expression of multiple mesenchymal markers including *Cdh2* (N-cadherin), *Des, Acta2* (SMA), and *Vim* as well as ECM genes including *Fn1, Col1a1, Col1a2*, and *Col3a1* in BALB/c *Ift88*^{Orpk} cholangiocytes compared to WT BALB/c cholangiocytes and C57BL/6 *Ift88*^{Orpk} cholangiocytes (Fig. 6D). These data suggest that BALB/c, but not C57BL/6, *Ift88*^{Orpk} cholangiocytes increase expression of profibrotic growth factor receptors and produce extracellular matrix in response to cytokines (TGFB1) produced by BALB/c Ly6c^{hi} infiltrating macrophages.

Analysis of receptors that drive cholangiocyte proliferation shows that *Ift88*^{Orpk} C57BL/6 cholangiocytes have increased expression of pro-proliferative receptors including the *Vegfc* receptor (*Flt4*) while *Ift88*^{Orpk} BALB/c cholangiocytes have decreased expression of receptors that promote cholangiocyte proliferation compared to their respective controls (Fig. 6E) [38]. Likewise, there is a downregulation of gene expression for receptors known to inhibit cholangiocyte proliferation in *Ift88*^{Orpk} C57BL/6 cholangiocytes and upregulation of these same pathways in *Ift88*^{Orpk} BALB/c cholangiocytes compared to controls (Fig. 6E). These data suggest that cholangiocytes from C57BL/6 *Ift88*^{Orpk} mice respond to proliferative cytokines including *Vegfc* (produced by Ly6c^{lo} infiltrating macrophages) due to the presence of the *Vegfc* receptor (*Flt4*) whereas BALB/c *Ift88*^{Orpk} cholangiocytes do not possess the receptors necessary to bind *Vegfc* and drive cholangiocyte proliferation.

Finally, to assess the interplay between cholangiocytes and infiltrating macrophages, we analyzed cholangiocyte RNA

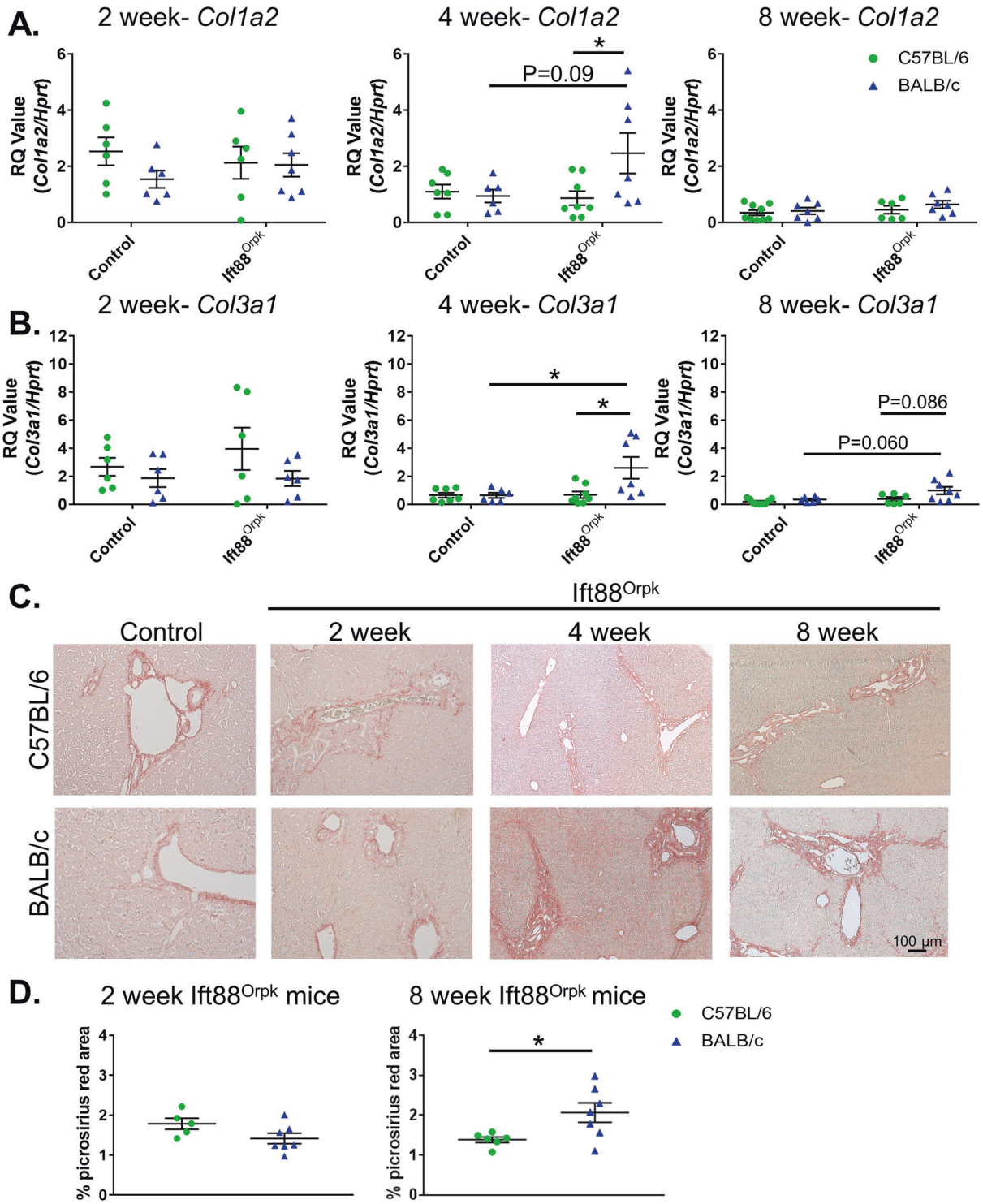

Fig. 4 BALB/c *Ift88*^{Orpk} mice have increased hepatic fibrosis compared to C57BL/6 *Ift88*^{Orpk} mice. A, **B** qRT-PCR analysis of (**A**) *Col1a2* and (**B**) *Col3a1* mRNA in whole liver tissue from 2, 4, and 8-week old control and *Ift88*^{Orpk} C57BL/6 and BALB/c mice. Data are shown as the average ± SE. *$P < 0.05$. **C** Control and *Ift88*^{Orpk} livers were harvested at the indicated time points and stained with picrosirius red. A representative 10X objective image from each mouse is shown. $N = 5–8$ per group. **D** Quantification of picrosirius red area for 2 and 8-week old C57BL/6 and BALB/c *Ift88*^{Orpk} mice are shown as average ± SE. *$P < 0.05$.

sequencing data for the expression of chemoattractants that might recruit Ly6c^{hi} infiltrating macrophages and other immune cells to the liver. Our analysis shows that BALB/c *Ift88*^{Orpk} cholangiocytes have increased expression of *Ccl2, Cxcl1*, *Cxcl2*, and *Csf1* compared to BALB/c WT mice and C57BL/6 *Ift88*^{Orpk} mice (Fig. 6F). In contrast, there was no overt upregulation of chemoattractant cytokines in cholangiocytes from C57BL/6 *Ift88*^{Orpk} mice, which agrees with data showing that C57BL/6 *Ift88*^{Orpk} mice do not have a significant increase in the number of Ly6c^{hi} macrophages compared to control C57BL/6 mice (Fig. 2). The lack of increased chemoattractant gene expression in C57BL/6 *Ift88*^{Orpk} mice may also explain why most of the infiltrating

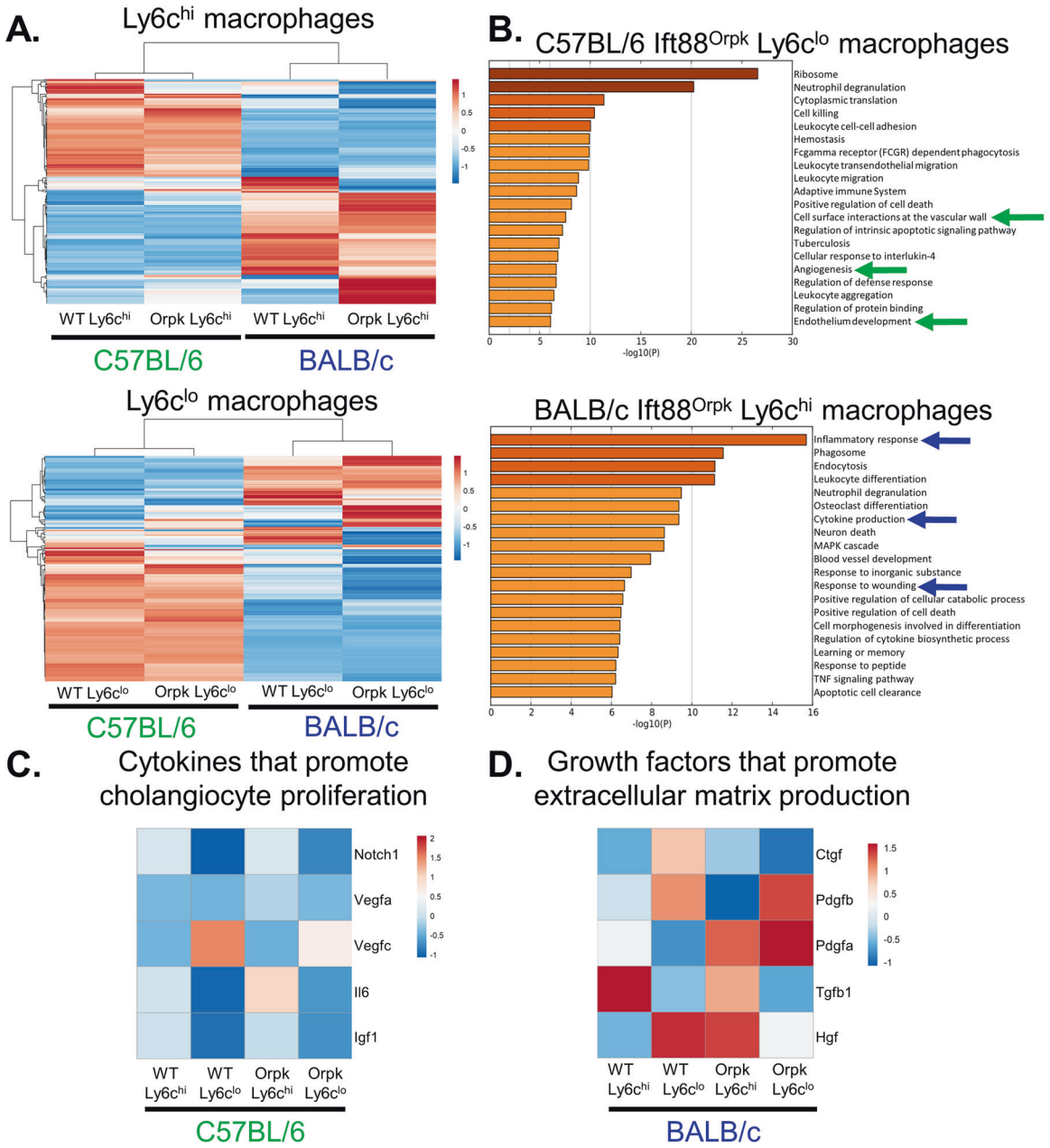

Fig. 5 BALB/c infiltrating macrophages express pro-fibrotic genes while C57BL/6 infiltrating macrophages express genes associated with cholangiocyte proliferation. A Heatmap analysis of RNA sequencing data obtained from 4-week old WT and *Ift88*^{Orpk} C57BL/6 and BALB/c mice. The top 200 DEGs for Ly6c^{hi} and Ly6c^{lo} macrophages are shown. **B** GO pathway analysis of the genes enriched in C57BL/6 Ly6^{lo} macrophages and BALB/c Ly6c^{hi} macrophages. Green arrows (top panel) indicate pathways containing genes associated with cholangiocyte proliferation and biliary hyperplasia. Blue arrows (bottom panel) indicate pathways containing genes associated with extracellular matrix production and fibrosis. **C**, **D** Heatmap analysis of RNA sequencing data from Ly6c^{hi} and Ly6c^{lo} macrophages showing expression of genes known to (**C**) promote cholangiocyte proliferation or (**D**) promote extracellular matrix production and fibrosis.

macrophages in this strain are Ly6c^{lo} (since they are unable to recruit in new, Ly6c^{hi} infiltrating macrophages from the circulation).

Blockade of Ly6c^{hi} infiltrating macrophage recruitment to the liver does not affect biliary hyperplasia or fibrosis in BALB/c *Ift88*^{Orpk} mice

To test whether BALB/c Ly6c^{hi} macrophages drive the fibrotic phenotype, we generated BALB/c *Ift88*^{Orpk} CCR2−/− (CCR2^{mut}) mice. These mice have a marked reduction in the number of Ly6c^{hi} macrophages in the liver due to their inability to emigrate out of the bone marrow in the absence of CCR2 [24]. Our data indicate that mice lacking CCR2 have significantly reduced numbers of Ly6c^{hi} macrophages in the liver in steady-state and in *Ift88*^{Orpk} mice compared to CCR2 control mice (Fig. 7A). In contrast, CCR2 deficiency did not significantly affect the number of Ly6c^{lo} macrophages in control or *Ift88*^{Orpk} mice (Fig. 7A).

To assess the impact of reduced Ly6c^{hi} infiltrating macrophages on fibrosis in BALB/c *Ift88*^{Orpk} mice, we performed the qRT-PCR analysis of mRNA isolated from whole liver tissue at 8 weeks of age. Surprisingly and in contrast to our initial hypothesis, the data indicate that *Col1a2* and *Col3a1* mRNA levels were not significantly different between BALB/c *Ift88*^{Orpk} CCR2^{Ctrl} and BALB/c *Ift88*^{Orpk} CCR2^{mut} mice (Fig. 7B). Likewise, quantification of

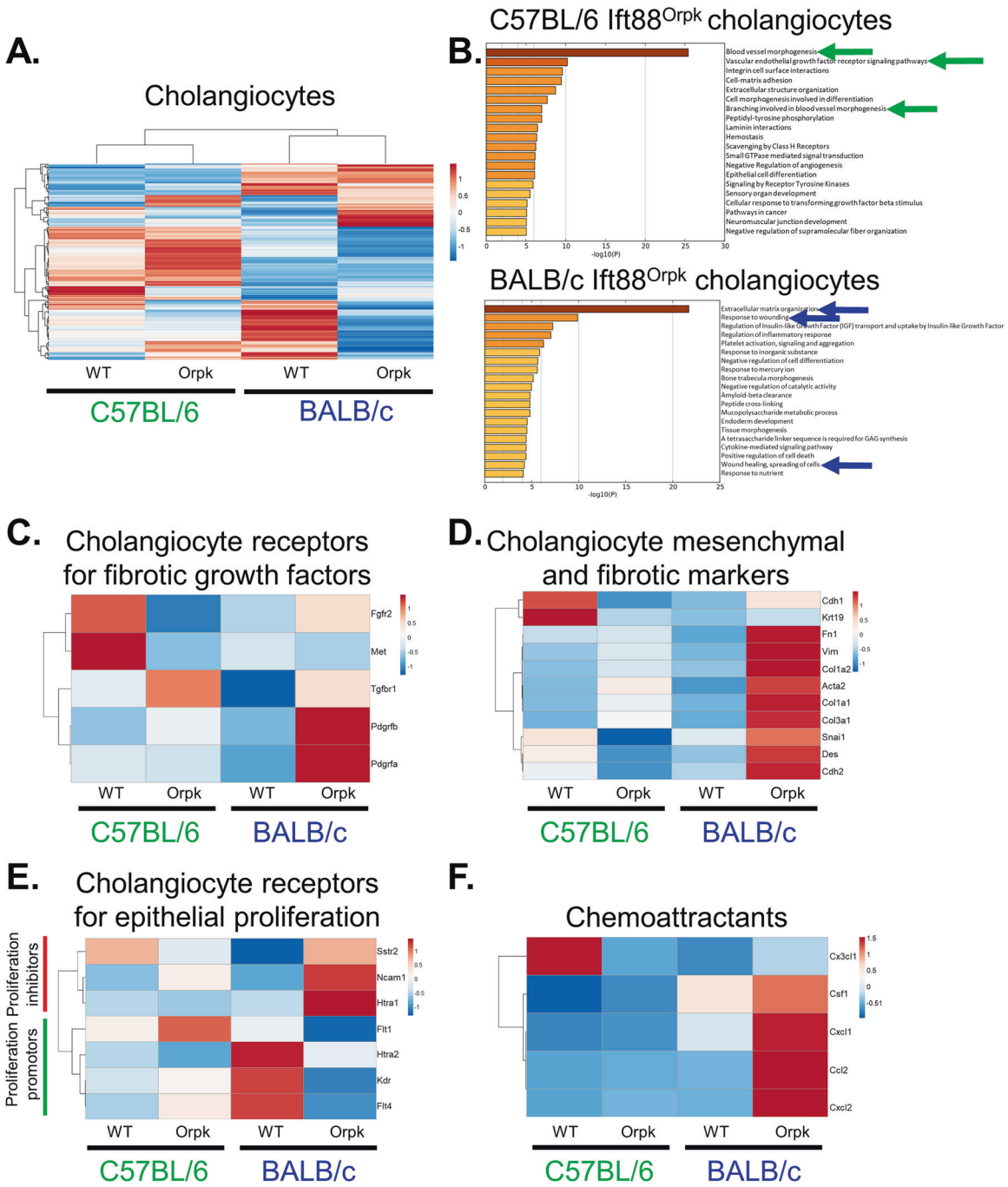

Fig. 6 BALB/c *Ift88*^{Orpk} cholangiocytes express genes associated with a mesenchymal and fibrotic phenotype while C57BL/6 *Ift88*^{Orpk} cholangiocytes express receptors associated with cholangiocyte proliferation. A Heatmap of the top 200 DEGs from WT and *Ift88*^{Orpk} cholangiocytes isolated from C57BL/6 and BALB/c mice. **B** GO pathway analysis of the genes enriched in C57BL/6 and BALB/c *Ift88*^{Orpk} cholangiocytes. Green arrows (top panel) indicate pathways containing genes associated with cholangiocyte proliferation and biliary hyperplasia. Blue arrows (bottom panel) indicate pathways containing genes associated with extracellular matrix production and fibrosis. **C**–**F** Heatmaps showing gene expression of (**C**) cholangiocyte receptors that bind to pro-fibrotic growth factors, (**D**) mesenchymal markers, (**E**) receptors known to promote or inhibit cholangiocyte proliferation, and (**F**) chemoattactants that promote immune cell recruitment. In panel (**E**), receptors that inhibit cholangiocyte proliferation are indicated by the red bar on the left side of the graph whereas receptors that promote cholangiocyte proliferation are indicated by a green bar on the left side of the graph.

picrosirius red-stained liver sections or analysis of hydroxyproline levels (a measure of total collagen protein [39]) shows no difference between BALB/c *Ift88*^{Orpk} CCR2^{Ctrl} and BALB/c *Ift88*^{Orpk} CCR2^{mut} mice (Fig. 7C).

Quantification of biliary hyperplasia and bile duct number from H&E stained sections shows that loss of Ly6c^{hi} macrophages does not affect the biliary phenotype in BALB/c *Ift88*^{Orpk} mice (Fig. 7D). Further, the number of cytokeratin 19+ cholangiocytes as assessed by flow cytometry (Fig. 7E) and the expression of *Krt19* mRNA did not differ between *Ift88*^{Orpk} CCR2^{Ctrl} and *Ift88*^{Orpk} CCR2^{mut} mice (Fig. 7F). These data show that while infiltrating macrophage subtypes correlate with phenotypic outcome, they do not directly cause the observed phenotypic differences between BALB/c and C57BL/6 *Ift88*^{Orpk} mice.

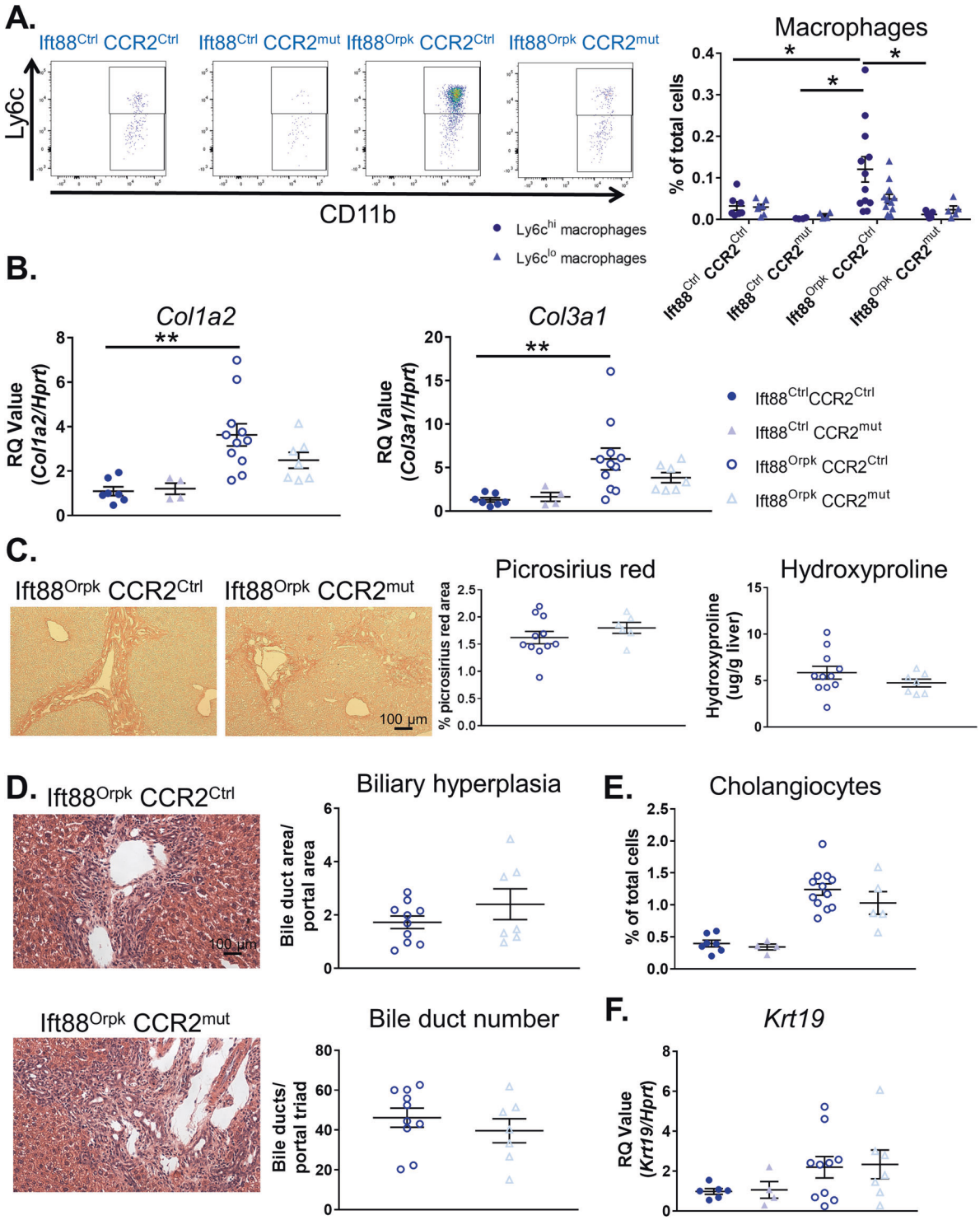

Fig. 7 Genetic inhibition of Ly6c^{hi} infiltrating macrophage recruitment to the liver does not affect biliary hyperplasia or fibrosis in BALB/c *Ift88^{Orpk}* mice. A Representative flow cytometry plots of Ly6c^{hi} and Ly6c^{lo} macrophages from 8-week-old BALB/c livers. Quantification of the number of Ly6c^{hi} and Ly6c^{lo} macrophages as a percentage of total cells is shown as the mean ± SE. *$P < 0.05$. **B** qRT-PCR data showing *Col1a2* and *Col3a1* gene expression in 8-week old BALB/c livers. Values represent the mean + SE. **$P < 0.01$. **C** Representative picrosirius red images from 8 weeks old BALB/c *Ift88^{Orpk}* CCR2^{Ctrl} vs *Ift88^{Orpk}* CCR2^{mut} mice. Quantification of the percentage picrosirius red positive area is shown as the mean ± SE. Also shown is the quantification of hydroxyproline content (µg/g liver tissue) isolated from *Ift88^{Orpk}* CCR2^{Ctrl} vs *Ift88^{Orpk}* CCR2^{mut} mice. **D** Representative H&E stained sections from 8-week-old BALB/c *Ift88^{Orpk}* CCR2^{Ctrl} vs *Ift88^{Orpk}* CCR2^{mut} mice. Quantification of biliary hyperplasia (bile duct area/portal area) and bile duct number is shown as the mean ± SE. **E** Quantification of the number of cytokeratin 19 + (K19 +) cholangiocytes as determined by flow cytometry. Values represent the mean ± SE. **F** qRT-PCR data showing the expression level of *Krt19* mRNA from 8-week-old BALB/c CCR2 mice. Values represent the mean ± SE.

DISCUSSION

Patients with HRFCD present with variable levels of inflammation, cyst progression, and fibrosis despite a common underlying genetic mutation suggesting that both extrinsic environmental and intrinsic genetic alterations may influence the rate and severity of disease progression. Herein, we use *Ift88*^{Orpk} mice on different, inbred genetic backgrounds to test the hypothesis that the subtype of infiltrating macrophage in the liver is a major determinant of phenotypic outcome. Although our data indicate a significant correlation between the subtype of infiltrating macrophages and the phenotypic outcome, Ly6c^{hi} infiltrating macrophages do not directly cause the increased fibrosis observed in BALB/c *Ift88*^{Orpk} mice. Despite the lack of causality, our data indicate that early differences in infiltrating macrophage phenotype may be predictive of long-term phenotypic outcome in the liver.

We observed a strong correlation between the subtype of infiltrating macrophage in the liver at the early stages of the disease and the phenotypic outcome at late stages. Quite surprisingly, we did not see an effect on phenotypic outcome when we blocked the infiltrating macrophage subtype (Ly6c^{hi}) that we proposed was driving the fibrotic outcome in BALB/c *Ift88*^{Orpk} mice. One possible reason for the lack of causality is that the effect of blocking Ly6c^{hi} infiltrating macrophage accumulation in BALB/c *Ift88*^{Orpk} mice may be hidden due to compensation by other inflammatory cells, such as Kupffer cells, producing pro-fibrotic growth factors. This possibility seems plausible due to the relative paucity of Ly6c^{hi} infiltrating macrophages in the liver in comparison to Kupffer cells. Despite the lack of a causative role, our data are still important as they indicate that infiltrating macrophage subtypes at early periods of the disease may be predictive of late-stage phenotypic outcomes in the liver.

Our data show that genetic strain has a strong influence on epithelial cell gene expression. During steady-state conditions, there is a moderate difference in the gene expression profile between WT C57BL/6 and BALB/c cholangiocytes. However, there is a clear difference in gene expression patterns between cholangiocytes isolated from C57BL/6 and BALB/c *Ift88*^{Orpk} mice despite the presence of a common genetic mutation. BALB/c *Ift88*^{Orpk} cholangiocytes display upregulate pro-fibrotic growth factor receptors and mesenchymal markers while downregulating receptors associated with epithelial cell proliferation. In contrast, C57BL/6 mice have no change in mesenchymal marker expression but upregulate receptors associated with epithelial proliferation. Why cholangiocytes express different receptors during disease settings despite a common genetic mutation remains to be determined.

Previous studies in the kidney [16, 18] and liver [17] indicate that global depletion of phagocytic cells using liposomal clodronate ameliorated HRFCD pathology. Since Kupffer cells are the major phagocytic cell in the liver, and general depletion of phagocytic cells reduced liver hepatic fibrocystic disease [17], it is likely that these effects are the result of Kupffer cell depletion and not loss of infiltrating macrophages. It is also possible that other phagocytic cells such as liver dendritic cells (type I or type II) may be involved in regulating liver pathology. This is in good agreement with the data in this manuscript showing that, although correlative, Ly6c^{hi} infiltrating macrophages do not influence the liver phenotype in the *Ift88*^{Orpk} model of HRFCD. Future studies specifically targeting Kupffer cells or dendritic cells in mouse models of HRFCD are needed to test this hypothesis.

Overall, our data show that genetic strain impacts infiltrating macrophage subtype, gene expression, and phenotypic outcome, although the effect on phenotypic outcome is not dependent on the subset of infiltrating macrophage present in the liver. Therefore, while targeting specific subsets of macrophage may be beneficial in regards to renal fibrocystic disease [27, 28], this does not appear to be the case in the liver.

DATA AVAILABILITY

The datasets used and/or analyzed during the current study are available from the corresponding author on reasonable request.

REFERENCES

1. Wilson PD. Polycystic kidney disease. N Engl J Med. 2004;350:151–64.
2. Yoder BK, Richards WG, Sweeney WE, Wilkinson JE, Avener ED, Woychik RP. Insertional mutagenesis and molecular analysis of a new gene associated with polycystic kidney disease. Proc Assoc Am Phys. 1995;107:314–23.
3. Yoder BK, Richards WG, Sommardahl C, Sweeney WE, Michaud EJ, Wilkinson JE, et al. Differential rescue of the renal and hepatic disease in an autosomal recessive polycystic kidney disease mouse mutant. A new model to study the liver lesion. Am J Pathol. 1997;150:2231–41.
4. Woon C, Bielinski-Bradbury A, O'Reilly K, Robinson P. A systematic review of the predictors of disease progression in patients with autosomal dominant polycystic kidney disease. BMC Nephrol. 2015;16:140.
5. Cnossen WR, te Morsche RH, Hoischen A, Gilissen C, Chrispijn M, Venselaar H, et al. Whole-exome sequencing reveals LRP5 mutations and canonical Wnt signaling associated with hepatic cystogenesis. Proc Natl Acad Sci USA. 2014;111:5343–8.
6. Janssen MJ, Salomon J, Cnossen WR, Bergmann C, Pfundt R, Drenth JP. Somatic loss of polycystic disease genes contributes to the formation of isolated and polycystic liver cysts. Gut. 2015;64:688–90.
7. D'Agnolo HM, Drenth JP. Risk factors for progressive polycystic liver disease: where do we stand? Nephrol Dial Transpl. 2016;31:857–9.
8. Hou X, Mrug M, Yoder BK, Lefkowitz EJ, Kremmidiotis G, D'Eustachio P, et al. Cystin, a novel cilia-associated protein, is disrupted in the cpk mouse model of polycystic kidney disease. J Clin Investig. 2002;109:533–40.
9. Bearoff F, Del Rio R, Case LK, Dragon JA, Nguyen-Vu T, Lin CY, et al. Natural genetic variation profoundly regulates gene expression in immune cells and dictates susceptibility to CNS autoimmunity. Genes Immunol. 2016;17:386–95.
10. Raj T, Rothamel K, Mostafavi S, Ye C, Lee MN, Replogle JM, et al. Polarization of the effects of autoimmune and neurodegenerative risk alleles in leukocytes. Science. 2014;344:519–23.
11. Naranbhai V, Fairfax BP, Makino S, Humburg P, Wong D, Ng E, et al. Genomic modulators of gene expression in human neutrophils. Nat Commun. 2015;6:7545.
12. Zeier M, Fehrenbach P, Geberth S, Mohring K, Waldherr R, Ritz E. Renal histology in polycystic kidney disease with incipient and advanced renal failure. Kidney Int. 1992;42:1259–65.
13. Cowley BD Jr., Gudapaty S, Kraybill AL, Barash BD, Harding MA, Calvet JP, et al. Autosomal-dominant polycystic kidney disease in the rat. Kidney Int. 1993;43:522–34.
14. Mrug M, Zhou J, Woo Y, Cui X, Szalai AJ, Novak J, et al. Overexpression of innate immune response genes in a model of recessive polycystic kidney disease. Kidney Int. 2008;73:63–76.
15. Ta MH, Harris DC, Rangan GK. Role of interstitial inflammation in the pathogenesis of polycystic kidney disease. Nephrology. 2013;18:317–30.
16. Swenson-Fields KI, Vivian CJ, Salah SM, Peda JD, Davis BM, van Rooijen N, et al. Macrophages promote polycystic kidney disease progression. Kidney Int. 2013;83:855–64.
17. Locatelli L, Cadamuro M, Spirli C, Fiorotto R, Lecchi S, Morell CM, et al. Macrophage recruitment by fibrocystin-defective biliary epithelial cells promotes portal fibrosis in congenital hepatic fibrosis. Hepatology. 2016;63:965–82.
18. Karihaloo A, Koraishy F, Huen SC, Lee Y, Merrick D, Caplan MJ, et al. Macrophages promote cyst growth in polycystic kidney disease. J Am Soc Nephrol. 2011;22:1809–14.
19. Yang Y, Chen M, Zhou J, Lv J, Song S, Fu L, et al. Interactions between macrophages and cyst-lining epithelial cells promote kidney cyst growth in Pkd1-deficient mice. J Am Soc Nephrol. 2018;29:2310–25.
20. Ginhoux F, Schultze JL, Murray PJ, Ochando J, Biswas SK. New insights into the multidimensional concept of macrophage ontogeny, activation and function. Nat Immunol. 2016;17:34–40.
21. Schulz C, Gomez Perdiguero E, Chorro L, Szabo-Rogers H, Cagnard N, Kierdorf K, et al. A lineage of myeloid cells independent of Myb and hematopoietic stem cells. Science. 2012;336:86–90.
22. Matsushima K, Larsen CG, DuBois GC, Oppenheim JJ. Purification and characterization of a novel monocyte chemotactic and activating factor produced by a human myelomonocytic cell line. J Exp Med. 1989;169:1485–90.
23. Furuichi K, Wada T, Iwata Y, Kitagawa K, Kobayashi K, Hashimoto H, et al. CCR2 signaling contributes to ischemia-reperfusion injury in kidney. J Am Soc Nephrol. 2003;14:2503–15.
24. Seki E, de Minicis S, Inokuchi S, Taura K, Miyai K, van Rooijen N, et al. CCR2 promotes hepatic fibrosis in mice. Hepatology. 2009;50:185–97.
25. Miura K, Yang L, van Rooijen N, Ohnishi H, Seki E. Hepatic recruitment of macrophages promotes nonalcoholic steatohepatitis through CCR2. Am J Physiol Gastrointest Liver Physiol. 2012;302:G1310–21.

26. Zimmerman KA, Song CJ, Gonzalez-Mize N, Li Z, Yoder BK. Primary cilia disruption differentially affects the infiltrating and resident macrophage compartment in the liver. Am J Physiol Gastrointest Liver Physiol. 2018;314:G677–89.
27. Viau A, Bienaime F, Lukas K, Todkar AP, Knoll M, Yakulov TA et al. Cilia-localized LKB1 regulates chemokine signaling, macrophage recruitment, and tissue homeostasis in the kidney. EMBO J. 2018 https://doi.org/10.15252/embj.201798615.
28. Cassini MF, Kakade VR, Kurtz E, Sulkowski P, Glazer P, Torres R et al. Mcp1 promotes macrophage-dependent cyst expansion in autosomal dominant polycystic kidney disease. J Am Soc Nephrol. 2018 https://doi.org/10.1681/ASN.2018050518.
29. Zoja C, Corna D, Locatelli M, Rottoli D, Pezzotta A, Morigi M, et al. Effects of MCP-1 inhibition by bindarit therapy in a rat model of polycystic kidney disease. Nephron. 2015;129:52–61.
30. Falix FA, Weeda VB, Labruyere WT, Poncy A, de Waart DR, Hakvoort TB, et al. Hepatic Notch2 deficiency leads to bile duct agenesis perinatally and secondary bile duct formation after weaning. Dev Biol. 2014;396:201–13.
31. Dobin A, Davis CA, Schlesinger F, Drenkow J, Zaleski C, Jha S, et al. STAR: ultrafast universal RNA-seq aligner. Bioinformatics. 2013;29:15–21.
32. Anders S, Pyl PT, Huber W. HTSeq-a Python framework to work with high-throughput sequencing data. Bioinformatics. 2015;31:166–9.
33. Ramachandran P, Pellicoro A, Vernon MA, Boulter L, Aucott RL, Ali A, et al. Differential Ly-6C expression identifies the recruited macrophage phenotype, which orchestrates the regression of murine liver fibrosis. Proc Natl Acad Sci USA. 2012;109:E3186–3195.
34. Means AL, Xu Y, Zhao A, Ray KC, Gu G. A CK19(CreERT) knockin mouse line allows for conditional DNA recombination in epithelial cells in multiple endodermal organs. Genesis. 2008;46:318–23.
35. Amura CR, Brodsky KS, Groff R, Gattone VH, Voelkel NF, Doctor RB. VEGF receptor inhibition blocks liver cyst growth in pkd2(WS25/-) mice. Am J Physiol Cell Physiol. 2007;293:C419–428.
36. Dooley S, ten Dijke P. TGF-beta in progression of liver disease. Cell Tissue Res. 2012;347:245–56.
37. Ying HZ, Chen Q, Zhang WY, Zhang HH, Ma Y, Zhang SZ, et al. PDGF signaling pathway in hepatic fibrosis pathogenesis and therapeutics (review). Mol Med Rep. 2017;16:7879–89.
38. Hall C, Sato K, Wu N, Zhou T, Kyritsi K, Meng F, et al. Regulators of cholangiocyte proliferation. Gene Expr. 2017;17:155–71.
39. Samuel CS. Determination of collagen content, concentration, and sub-types in kidney tissue. Methods Mol Biol. 2009;466:223–35.

ACKNOWLEDGEMENTS

We would like to thank members of Dr. Yoder's laboratory for helpful suggestions during these studies. The authors would also like to acknowledge Mandy J. Croyle for her technical assistance.

AUTHOR CONTRIBUTIONS

KAZ designed the research studies. CJS, KAZ, EJGA, SJB, AY, JZ, and ZL, conducted experiments and acquired data. KAZ, EJGA, SJB, AY, MM, DKC, MC, and BKY analyzed the data. BKY, KAZ, and MM provided reagents. KAZ wrote the manuscript. All authors reviewed the manuscript.

FUNDING

Funding for these studies was provided by: PKD foundation grant 214g16a (BKY); UAB School of Medicine AMC21 grant (BKY, MM); K01DK119375 (KAZ), National Institutes of Health T32 training grant in Basic Immunology and Immunologic disease 2T32AI007051-38 (KAZ), a Pilot and Feasibility Grants from the Baltimore PKD Center 2P30DK090868 (KAZ), a pilot grant from the UAB Hepato/Renal Fibrocystic Disease Core Center 5P30DK074038 (KAZ), a seed grant from the Presbyterian Health Foundation (KAZ), and a pilot grant from the Oklahoma Center for Microbial Pathogenesis and Immunity COBRE(1P20GM134973) to KAZ, R01 DK115752 (BKY), R01 DK097423 (MM), and 1-I01-BX00229, Department of Veterans Affairs (MM). The following NIH-funded cores provided services for this project: UAB Hepato/Renal Fibrocystic Disease Core Center P30-DK074038, UAB-UCSD O'Brien Center for Acute Kidney Injury Research P30-DK079337, and the UAB Comprehensive Flow Cytometry Core P30-AR048311 and P30-AI27667. Additional services were provided by the UAB comparative pathology lab and UAB Heflin Genomics Core.

COMPETING INTEREST

The authors declare no competing interests.

ETHICS APPROVAL AND CONSENT TO PARTICIPATE

This study does not require ethics approval and consent to participate.

ADDITIONAL INFORMATION

Correspondence and requests for materials should be addressed to B.K.Y.

Reprints and permission information is available at http://www.nature.com/reprints

Publisher's note Springer Nature remains neutral with regard to jurisdictional claims in published maps and institutional affiliations.